

Spectroscopic Survey of γ Doradus Stars

I. Comprehensive atmospheric parameters and abundance analysis of γ Doradus stars

F. Kahraman Alıçavuş^{1,2*}, E. Niemczura², P. De Cat³, E. Soyduğan¹,
 Z. Kołaczkowski², J. Ostrowski², J. H. Telting⁴, K. Uytterhoeven^{5,6}, E. Poretti⁷,
 M. Rainer⁷, J. C. Suárez⁸, L. Mantegazza⁷, P. Kilmartin⁹ and K. R. Pollard⁹

¹Faculty of Sciences and Arts, Physics Department, Canakkale Onsekiz Mart University, 17100, Canakkale, Turkey

²Instytut Astronomiczny, Uniwersytet Wrocławski, Kopernika 11, 51-622 Wrocław, Poland

³Royal observatory of Belgium, Ringlaan 3, B-1180 Brussel, Belgium

⁴Nordic Optical Telescope, Rambla José Ana Fernández Pérez 7, 38711 Breña Baja, Spain

⁵Instituto de Astrofísica de Canarias, E-38205 La Laguna, Tenerife, Spain

⁶Universidad de La Laguna, Departamento de Astrofísica, E-38206 La Laguna, Tenerife, Spain

⁷INAF-Osservatorio Astronomico di Brera, Via Bianchi 46, I-23807 Merate, Italy

⁸Department Física Teórica y del Cosmos. Universidad de Granada. Campus de Fuentenueva, 18071. Granada. Spain

⁹Department of Physics and Astronomy, University of Canterbury, Private Bag 4800, Christchurch, New Zealand

Accepted ... Received ...; in original form ...

ABSTRACT

We present a spectroscopic survey of known and candidate γ Doradus stars. The high-resolution, high signal-to-noise spectra of 52 objects were collected by five different spectrographs. The spectral classification, atmospheric parameters (T_{eff} , $\log g$, ξ), $v \sin i$ and chemical composition of the stars were derived. The stellar spectral and luminosity classes were found between G0-A7 and IV-V, respectively. The initial values for T_{eff} and $\log g$ were determined from the photometric indices and spectral energy distribution. Those parameters were improved by the analysis of hydrogen lines. The final values of T_{eff} , $\log g$ and ξ were derived from the iron lines analysis. The T_{eff} values were found between 6000 K and 7900 K, while $\log g$ values range from 3.8 to 4.5 dex. Chemical abundances and $v \sin i$ values were derived by the spectrum synthesis method. The $v \sin i$ values were found between 5 and 240 km s⁻¹. The chemical abundance pattern of γ Doradus stars were compared with the pattern of non-pulsating stars. It turned out that there is no significant difference in abundance patterns between these two groups. Additionally, the relations between the atmospheric parameters and the pulsation quantities were checked. A strong correlation between the $v \sin i$ and the pulsation periods of γ Doradus variables was obtained. The accurate positions of the analysed stars in the H-R diagram have been shown. Most of our objects are located inside or close to the blue edge of the theoretical instability strip of γ Doradus.

Key words: stars: general – stars: abundances – stars: chemically peculiar – stars: rotation – stars: variables: γ Doradus

1 INTRODUCTION

The class of γ Doradus (γ Dor) variables was defined by Balona, Krisciunas, & Cousins (1994) after discovery of the variability of the prototype of these pulsators (Cousins 1992; Krisciunas et al. 1993). The γ Dor variables exhibit pulsations in the non-radial, high-order (n), low-degree (l) grav-

ity modes with amplitudes at the level of 0.1 mag (V) and pulsation periods between 0.3 and 3 days (Kaye et al. 1999). The pulsations of γ Dor stars are driven by the mechanism of convective flux blocking (Guzik et al. 2000; Dupret et al. 2005). In the Hertzsprung-Russell (H-R) diagram, the theoretical instability strip of γ Dor variables is located partially inside the instability strip of δ Scuti (δ Sct) stars. In this small overlapping part, the existence of stars pulsating simultaneously in both δ Sct and γ Dor modes was predicted

* E-mail: filizkahraman01@gmail.com

(Dupret et al. 2004). These stars are called γ Dor/ δ Sct or A-F type hybrids. The γ Dor variables are A7-F5 dwarfs and/or sub-dwarfs (Kaye et al. 1999). This means that in the H-R diagram they are situated inside the region of the transition from a convective envelope to a convective core. In order to reveal properties of the pulsation mechanism in F type stars and to decide on the correct location of the theoretical instability strip of γ Dor stars in the H-R diagram the interaction between convection and pulsation has to be taken into account (Saio et al. 2015). Moreover, the investigation of γ Dor variables allows us to examine important subjects of the internal structure and evolution of intermediate mass stars (Miglio et al. 2008). In particular, the frequency spacing detected in the photometric time series has allowed the study of the internal structure and surface-to-core rotation (e.g. Kurtz et al. 2014; Van Reeth et al. 2015).

In-depth studies of the pulsating A-F type stars have now become possible due to the space observations. In particular, the high-precision light curves of the *Kepler* mission enabled investigation of many new A-F type variables (Borucki et al. 2010). Before the space observations, approximately 100 γ Dor stars were known (Henry, Fekel, & Henry 2011). The analysis of the *Kepler* data revealed many new candidate γ Dor, δ Sct and A-F type hybrid stars (Uytterhoeven et al. 2011; Grigahcène et al. 2010). The investigation of *Kepler* observations and ground-based photometric data allow us to determine pulsation characteristics, ranges of fundamental parameters, and position of these variables in the H-R diagram.

However, many new questions about the properties of the γ Dor stars, δ Sct stars and their hybrids arose. The first question concerns the exact location of the instability domains of these variables in the H-R diagram. According to the existing studies, there seems to be no clear distinction in the edges of the observational instability strip of γ Dor and δ Sct stars. Moreover, it was shown that candidate hybrids of γ Dor and δ Sct stars were detected everywhere inside the theoretical instability strips of both types of pulsating stars (e.g. Kurtz et al. 2014; Niemczura et al. 2015). Another question relates to the chemical structure of the hybrid stars. Some Am hybrid stars were discovered, and these results showed that a relation between the Am phenomenon and hybridity could exist (Hareter et al. 2011). Solving these problems requires investigation of whether chemical and physical differences between hybrids, γ Dor, and δ Sct variables exist. Therefore, it is necessary to obtain the accurate physical and chemical characteristics of all classes of A-F type variables. Hence, reliable spectroscopic and multi-colour photometric studies are essential.

So far, several photometric and spectroscopic studies of γ Dor stars have been carried out (e.g. Henry, Fekel, & Henry 2007; Mathias et al. 2004). One of the most detailed spectroscopic investigations of γ Dor stars was presented by Bruntt, De Cat, & Aerts (2008). They derived fundamental atmospheric parameters and chemical composition of *bona-fide* and candidate γ Dor stars to search for links between γ Dor, Am and λ Boötis stars, but no relations were found. Additionally, detailed spectroscopic analyses of γ Dor stars detected in satellite fields have been carried out (e.g. Tkachenko et al. 2012, 2013 a; Niemczura et al. 2015; Van Reeth et al. 2015). In

these studies, the fundamental atmospheric parameters and chemical abundances of these variables were derived.

The aim of this study is to obtain the atmospheric parameters and chemical abundances of some *bona-fide* and candidate γ Dor stars detected from the ground-based observations. Therefore, we gathered high-resolution and high signal-to-noise (S/N) spectra for 69 γ Dor stars using five different spectrographs from around the world. This sample contains a mixture of single stars, single-lined binaries (SB1) and double-lined spectroscopic binaries (SB2). The analysis of SB2 γ Dor stars will be presented in a separate paper (Kahraman Aliçavuş et al., in preparation). In this study, a detailed spectroscopic analysis of 52 single and SB1 γ Dor stars is performed. The high-resolution observation, data reduction and calibration details are given in Sect. 2. Spectral classification process is described in Sect. 3. Determination of the atmospheric parameters from photometric systems and spectral energy distribution are presented in Sect. 4. In Sect. 5, we introduce the atmospheric parameters determination from the analysis of hydrogen and iron lines, the detailed chemical abundance analysis, and discussion of the obtained parameters. The summary of the results and an outlook for future studies are given in Sect. 6.

2 OBSERVATIONS

The observations of our targets were carried out with five high-resolution spectrographs. Numbers of the observed single & SB1 and SB2 stars, observation years, spectral resolutions of instruments, wavelength range and signal-to-noise (S/N) ranges are given in Table 1. For each spectrograph, the listed S/N range gives the maximum and minimum value of S/N at 5500 Å. The following instruments were used in the survey:

- *FEROS* (Fibre-fed Extended Range Optical Spectrograph), an échelle spectrograph attached to the 2.2-m telescope of the European Southern Observatory (ESO, La Silla, Chile) (Elkin, Kurtz, & Nitschelm 2012);
- *FIES* (Fibre-fed Échelle Spectrograph), a cross-dispersed high-resolution échelle spectrograph attached to the 2.56-m Nordic Optical Telescope of the Roque de los Muchachos Observatory (ORM, La Palma, Spain) (Telting et al. 2014);
- *HARPS* (High Accuracy Radial Velocity Planet Searcher), an échelle spectrograph attached to the 3.6-m telescope of the European Southern Observatory (ESO, La Silla, Chile) (Mayor et al. 2003);
- *HERCULES* (High Efficiency and Resolution Canterbury University Large Échelle Spectrograph), a fibre-fed échelle spectrograph attached to the 1-m McLellan telescope of the Mt. John University Observatory (MJUO, Mount John, New Zealand) (Hearnshaw et al. 2003);
- *HERMES* (High Efficiency and Resolution Mercator Échelle Spectrograph), a high-resolution fibre-fed échelle spectrograph attached to the 1.2-m Mercator telescope at the Roque de los Muchachos Observatory (ORM, La Palma, Spain) (Raskin et al. 2011).

The collected spectra have been reduced and calibrated using the dedicated reduction pipelines of the instruments. The usual reduction steps for échelle spectra were applied,

Table 1. Information about the spectroscopic observations.

Instrument	Number of single & SB1/SB2 stars	Years of observations	Resolving power	Spectral range [Å]	S/N range
FEROS	0 / 8	2008	48000	3500-9200	170 - 340
FIES	29 / 2	2007-2010	67000	3700-7300	100 - 330
HARPS	11 / 4	2009-2011	80000	3780-6910	130 - 360
HERCULES	11 / 3	2007-2010	70000	4000-8800	110 - 300
HERMES	1 / 0	2010	85000	3770-9000	150

i.e.: bias subtraction, flat-field correction, removal of scattered light, order extraction, wavelength calibration, and merging of the orders. For the HERCULES data, an additional procedure had to be used to merge the échelle orders. In this procedure the overlapping parts of the orders were averaged using the signal-to-noise of the given order as the weight. The normalisation of all spectra was performed manually by using the *continuum* task of the NOAO/IRAF package¹.

Some of the studied stars were observed by more than one instrument. In this case, only the spectra of the instrument with the highest resolution were analysed. For some of the stars we collected more than one spectrum from the same instrument. For these stars all the spectra were combined and the average spectrum was investigated.

We collected the spectroscopic observations of both single-lined (single stars and SB1 binaries) and double-lined (SB2 binaries) stars. Some of these spectroscopic binaries had already been known in the literature as SB2 objects. In our sample, four new SB2 systems were detected: HD 85693, HD 155854, HD 166114 and HD 197187. The number of spectra we have so far for these targets is insufficient to determine their orbits. In this paper, we present the spectroscopic analysis of single and single lined spectroscopic binaries (SB1) only. An overview of the analysed objects is given in Table 2.

3 SPECTRAL CLASSIFICATION

A spectral classification gives crucial information about chemical peculiarity and initial atmospheric parameters of a star. Determination of the spectral type and the luminosity class relies on a comparison of the spectra of the studied stars with those of well-known standards, taking into account important hydrogen and metal lines.

As the γ Dor stars are late-A to mid-F type stars, we used only the spectra of standard A and F type stars from Gray et al. (2003) in the classification process. For each star, the spectral type determination was carried out three times, each time based on a different set of lines:

- (1) *Hydrogen lines*: $H\gamma$ and $H\delta$ lines,
- (2) *Metal lines*: Fe I, Ca I and Mg I and their ratios with the Balmer lines,
- (3) *Ca II K line* (stars earlier than F3) or *G-band* (for late F type stars).

In the case of a non-chemically peculiar star, all three methods should give the same result. However, for chemically

peculiar Am or λ Boötis stars, different spectral types are obtained from different sets of lines (Gray & Corbally 2009).

To obtain luminosity classes, we used blended lines of ionised iron and titanium near 4500 Å (Gray & Corbally 2009). In the case of A and early F type stars, Balmer lines are good indicators of the luminosity class while the G-band can be used for late F type stars. The luminosity classes were determined using all these indicators.

The resulting spectral types and luminosity classes are given in Table 2. They range between A7 and G0, and between IV and V, respectively. In the classification process, we discovered two mild Am stars, showing a difference of less than five spectral subtypes in the results based on the metal lines and the Ca II K line: HD 33204 (kA7 hA7 mF2 V) and HD 46304 (kA7 hA8 mF0 V). These mild Am stars are denoted as 'Am:' in Table 2. HD 33204 was already classified as an Am star (kA5 hA7 mF2) by Gray & Garrison (1989). We also found metal poor stars, exhibiting weak metal lines. These metal poor objects are indicated by 'm-*'. This notation represents the metallicity spectral class where '*' is a number: e.g. F2 m-2 means that metallicity spectral class of this star is F0 (Gray & Corbally 2009).

4 STELLAR PARAMETERS FROM PHOTOMETRY AND SED

Before the analysis of the high-resolution spectra, we derived initial values for atmospheric parameters of the stars using both different photometric indices (Sect. 4.1) and the SED method (Sect. 4.2). However, photometric colours and SEDs are very sensitive to the interstellar reddening ($E(B - V)$). Therefore, values of the interstellar reddening were first calculated using two different approaches.

In the first method, we used the interstellar extinction map code written by Dr. Shulyak (private information) based on the Galactic extinction maps published in Amôres & Lépine (2005). The $E(B - V)$ values from the extinction maps were calculated using the *Hipparcos* parallaxes (van Leeuwen 2007) and stellar galactic coordinates from the SIMBAD data base (Wenger et al. 2000)². Because of the lack of parallaxes for cluster members HD 22702 (Melotte 22 3308) and HD 169577 (NGC 6633 15), their distances were assumed as cluster distances, being 130 and 385 pc (Kharchenko et al. 2005), respectively.

In the second method, we derived $E(B - V)$ values from interstellar sodium lines. This approach is based on the relation between the equivalent width of the Na D₂ line

¹ <http://iraf.noao.edu/>

² <http://simbad.u-strasbg.fr/simbad/>

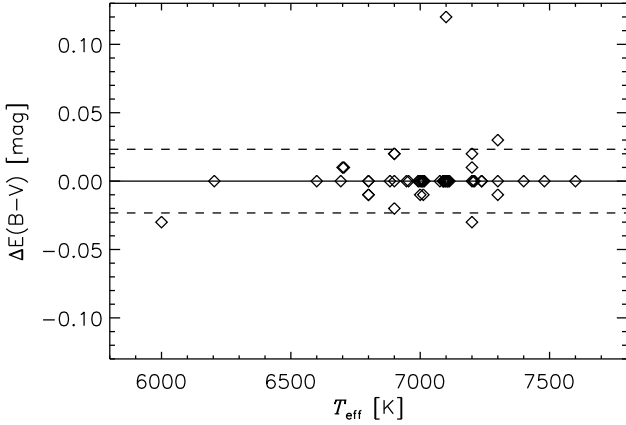


Figure 1. The differences between the $E(B - V)$ values derived from interstellar maps and the sodium NaD_2 lines. The dashed lines show $1-\sigma$ level.

(5889.95 Å) and the $E(B - V)$ value (Munari & Zwitter 1997).

The resulting $E(B - V)$ values obtained with both methods are listed in Table 3 and compared with each other in Fig. 1. Uncertainties of $E(B - V)$ values were adopted as equal 0.02 mag on the basis of the standard deviation resulting from the comparison of the values from two methods ($1-\sigma$, see Fig. 1). It can be seen that the results are consistent with each other, except for HD 169577. For this star, the difference between both values is about 0.1 mag. Note that for this star we used the NGC 6633 cluster distance in our calculation (first method). For the determination of stellar parameters, the average $E(B - V)$ values of both methods were used.

4.1 Photometric parameters

The effective temperatures T_{eff} and surface gravities $\log g$ of our targets were determined from photometric indices. These photometric parameters serve as input values for further analysis. We used $wby\beta$ Strömgren, Johnson, Geneva and 2MASS photometric data gathered from the General Catalogue of Photometric Data (Mermilliod, Mermilliod, & Hauck 1997) and the 2MASS catalogue (Cutri et al. 2003).

For 49 stars the atmospheric parameters T_{eff} and $\log g$ were estimated from the $wby\beta$ system. These parameters were acquired using the method of Moon & Dworetzky (1985), based on the V , $(b - y)$, m_1 , c_1 and β indices.

For 23 stars, Geneva photometry was used to derive the T_{eff} and $\log g$ values. The calculations were performed using the Künzli et al. (1997) calibration based on the $B2 - V1$, d and $m2$ indices.

Johnson $(B - V)$ colour indices were used to determine the T_{eff} of all studied stars. We applied the $(B - V)$ colour-temperature relation given by Sekiguchi & Fukugita (2000). For calculations of T_{eff} values, $\log g = 4.0$ and solar metallicities were assumed.

Finally, T_{eff} values of the stars were derived from the 2MASS photometry (Masana, Jordi, & Ribas 2006), using $(V - K)$ index. In the calculations, we assumed solar metallicity ($[m/H] = 0.0$) and $\log g = 4.0$ for all the stars.

The results obtained with all these methods are listed in Table 3. Uncertainties of the calculated T_{eff} and $\log g$ were estimated taking into account errors of photometric indices, reddening (0.02 mag, as discussed before), metallicity (0.1 dex), and surface gravity (0.1 dex), if it was necessary to assume this last parameter. Finally we derived the average uncertainties of T_{eff} and $\log g$ for each system (see Table 3). The average effective temperatures were calculated using the results from all considered photometric systems. In Fig. 2, these values are compared with individual results for each photometric system. The dashed lines represent the standard deviations of differences between the average temperatures and values from a given photometric system. These standard deviations are equal 125, 94, 96 and 140 K for $wby\beta$, Geneva, Johnson and 2MASS systems, respectively. As can be seen in Fig. 2, in most cases the obtained effective temperatures are consistent with the average values. In the case of $wby\beta$ the biggest difference was derived for HD 110379. This star is a binary system member, and its photometric colours can be influenced by the light from the second component.

Additionally, the $\log g$ values obtained from the $wby\beta$ and Geneva indices were compared with each other. The average $\log g$ value for the $wby\beta$ system is 4.08 dex while for the Geneva system, it reaches 4.32 dex. As can be inferred from these average values, surface gravities from $wby\beta$ are in general slightly lower than the Geneva ones.

4.2 Effective Temperature from SED

Stellar parameters can be estimated from the SED of a star. SEDs have to be constructed from spectrophotometry collected in different wavelengths, preferably from ultraviolet until infrared. Different parts of SED are sensitive to different stellar parameters. We used SEDs to obtain T_{eff} values, using the code written by Dr. Shulyak (private information). This code automatically searches for spectrophotometric observations from different data bases. Several data bases are available with the code, e.g. Adelman et al. (1989), Breger (1976), Alekseeva et al. (1996), Burnashev (1985) and Glushneva et al. (1992) covering the near-UV, visual, and near-IR wavelengths. The code can additionally use data from the Space Telescope Imaging Spectrograph (STIS; Hubble Space Telescope; Woodgate et al. 1998), the International Ultraviolet Explorer (IUE; Wamsteker et al. 2000), and the Ultraviolet Sky Survey Telescope (TD1; Boksenberg et al. 1973; Thompson et al. 1978). These archives cover the ultraviolet part of SED. The code allows also to input indices manually, if necessary.

In this study, we generally used the photometric colours of the $wby\beta$, Geneva, Johnson, and 2MASS systems and the ultraviolet TD1 observations as input values. SEDs constructed from these observed spectrophotometric measurements were compared with theoretical energy distributions, calculated from the Kurucz's atmospheric models (ATLAS9 code, Kurucz 1993). In these calculations, the solar metallicity ($[m/H] = 0$) and the $\log g$ value of 4.0 dex were assumed. The obtained T_{eff} values and their uncertainties are listed in Table 3. The average error is about 110 K. Differences between the obtained SED T_{eff} values and the average photometric values are shown in Fig. 2. In the figure dashed lines

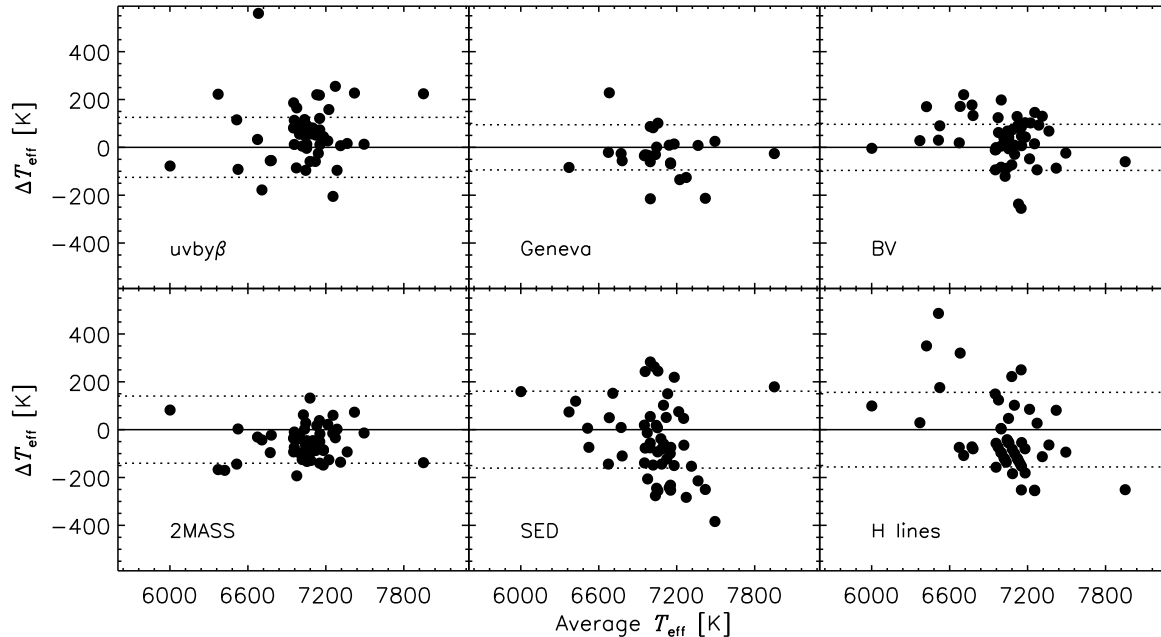


Figure 2. The differences between the average photometric effective temperatures and the T_{eff} obtained from photometric methods, SED and hydrogen lines. The dashed lines show 1- σ levels.

represent standard deviations of 160 K. As can be seen from Fig. 2, the highest difference was derived for HD 209295. This can be caused by the membership of this star to a binary system.

5 SPECTROSCOPIC ANALYSIS

In this section, the analysis of high-resolution and high S/N spectra is presented. Atmospheric parameters were derived from the analysis of hydrogen and metal lines. All the necessary atmospheric models were calculated with the ATLAS9 code (Kurucz 1993) that generates hydrostatic, plane-parallel and line-blanketed LTE (local thermodynamic equilibrium) models. The synthetic spectra were obtained with the SYNTHE code (Kurucz & Avrett 1981).

5.1 Analysis of hydrogen lines

The hydrogen lines analysis was applied to obtain the T_{eff} values of all stars. During the analysis of Balmer lines, the $\log g$ values were assumed to be 4.0 dex. Additionally, the solar metallicity and $v \sin i$ values were fixed during the analysis. The initial values of $v \sin i$ were taken from the approximate fitting of the synthetic spectra to the observed metal lines. The analysis was performed taking into account the $H\beta$, $H\gamma$ and $H\delta$ lines. The method proposed by Catanzaro, Leone, & Dall (2004) was applied. Initial T_{eff} values were taken from previous calculations, including photometric and the SED T_{eff} results. The final effective temperatures were derived minimizing the differences between synthetic and observed spectra. As an example, the result of the analysis for HD 23005 is shown in Fig. 3. As can be seen,

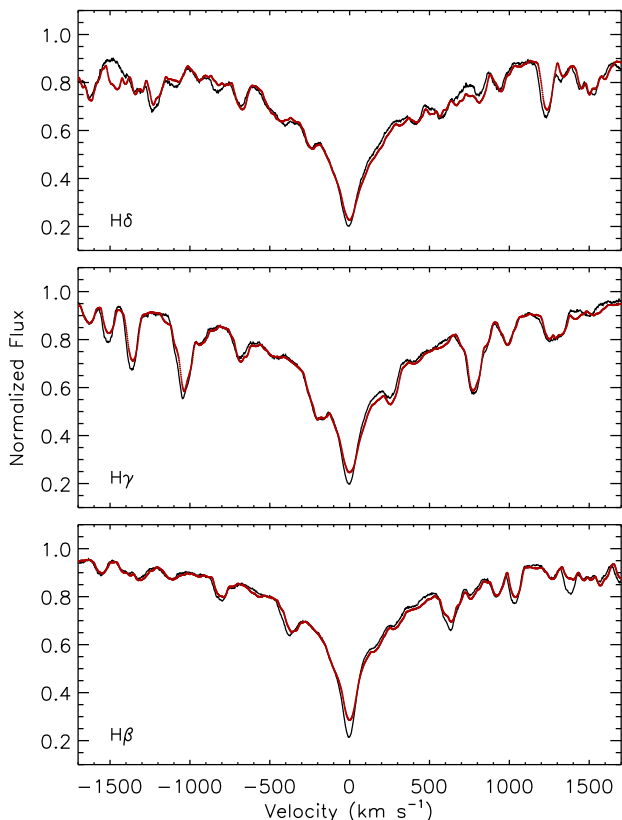


Figure 3. The observed Balmer lines (black lines) and the synthetic spectra (red lines) for HD 23005.

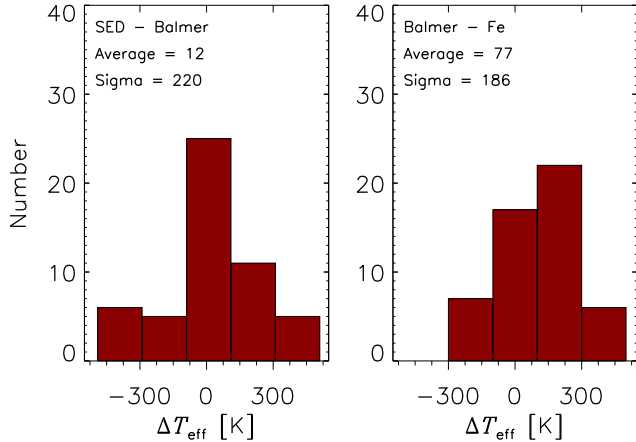


Figure 4. The distributions of differences between the effective temperatures determined from the hydrogen lines and SED analysis (left-hand panel) and from the hydrogen and Fe lines analysis (right-hand panel).

the observed hydrogen lines fit quite well with the synthetic spectra. The small deviations in the core of the lines are caused by the incorrect models, which are not able to explain Balmer line cores. The effective temperatures derived from the hydrogen lines and their uncertainties are listed in Table 4. These uncertainties were determined taking into account uncertainties resulting from quality of the spectra (S/N) and assumed values of $\log g$, $[m/H]$ and $v \sin i$. As known, the hydrogen lines are not sensitive to $\log g$ in the temperature range of γ Dor stars. Because of this, the $\log g$ parameter has no significant effect on T_{eff} values in our analysis (Smalley et al. 2002; Smalley 2005). The obtained uncertainties are in the range of ~ 150 -260 K.

In Fig. 2 the obtained values are compared with the average T_{eff} calculated from photometric indices. Standard deviation of these differences is about 200 K, and is shown by the dashed lines in Fig. 2. In Fig. 4 T_{eff} parameters from hydrogen lines are compared with the results of SED and iron lines analysis. The results are consistent within the error bars. Standard deviations and average values of these distributions are given in Fig. 4.

5.2 Atmospheric parameters from iron lines analysis

When T_{eff} and $\log g$ values were determined from photometric methods, SEDs and hydrogen lines, the iron lines analysis was performed assuming previously determined parameters as inputs. The initial analysis of the stellar $v \sin i$ values, revealed slowly and fast rotating stars in our sample. High rotation velocity causes that most of the spectral lines are blended. To analyse such spectra and to determine atmospheric parameters (T_{eff} , $\log g$ and microturbulent velocity ξ) the spectrum synthesis is the most appropriate method. To perform our analysis, we followed the same procedure as described in Niemczura et al. (2015). The values of T_{eff} , $\log g$ and ξ were determined taking into account Fe I and Fe II lines. T_{eff} and ξ parameters are highly sensitive to the strength of the Fe I lines while the $\log g$ parameter is almost totally insensitive to it. The strength of the Fe II lines is slightly affected by T_{eff} and ξ , but depends considerably

on the $\log g$. Considering the mentioned dependence of the iron lines on atmospheric parameters, we first obtained ξ values by looking at the correlation between the Fe I lines depths and abundances. Secondly, T_{eff} values were derived by checking the correlation between the excitation potential and the abundances calculated from individual Fe I lines. In both cases the correlations should be nearly zero, which means that for the proper atmospheric parameters of a star, the same iron abundance should be obtained from all iron lines. The surface gravity values were determined using the ionization balance of the Fe I and Fe II lines.

In Fig. 5, we show the distributions of the derived iron abundances (left), excitation potentials versus Fe I abundances (middle) and Fe I lines depths versus abundances (right) for the star HD 126516. Additionally, two sets of the atmospheric parameters for which the iron abundances were calculated are shown. The upper panels show these relations for the wrong atmospheric parameters, whereas the lower panels demonstrate the right solution. As we expect that for the correct parameters all iron lines give the same iron abundance within the error bars, it is clear that the smallest correlations of line strength, excitation potential, and obtained abundances indicate the correct solution.

The derived values for T_{eff} , $\log g$ and ξ together with their uncertainties are given in Table 4. The errors of the analysed parameters were obtained taking into account the effect of other parameters on the considered one. The lowest errors of 100 K for T_{eff} , 0.1 dex for $\log g$, and 0.1 km s^{-1} for ξ result from the steps adopted in the calculated stellar atmospheric models and synthetic spectra.

5.3 Abundances analysis

After the determination of T_{eff} , $\log g$ and ξ , chemical abundance analysis was carried out. In the first step, the spectra of each star were divided into the parts which widths depend mainly on $v \sin i$. For slowly rotating stars, parts covering only one or a few blended spectral features were selected. For moderate and fast rotating stars broader spectral ranges, including blends of many lines, were used. All parts were re-normalised by comparison with theoretical spectra, if necessary. Then the line identification for selected regions was performed using the line list of Kurucz³ (Kurucz & Bell 1995) taking into account only these elements that are most important in the given region. The abundance analysis was carried out by the spectrum synthesis method, which allowed us to determine chemical abundances and $v \sin i$ values at the same time. We used the classical least square method. Minimum differences between the observed and synthetic spectra indicate the final solution. After carrying out calculations for each spectral part of a given star, the average values of $v \sin i$ and chemical abundances were derived. The results are presented in Table 4 ($v \sin i$ and iron abundances) and Table 5 (chemical abundances and standard deviations).

The uncertainties of chemical elements given in Table 5 are standard deviations. The real errors of the elements include the effects of assumptions adopted to build the model of the atmosphere and uncertainties of atmospheric parameters (T_{eff} , $\log g$, ξ). The assumptions like

³ kurucz.harvard.edu/linelists.html

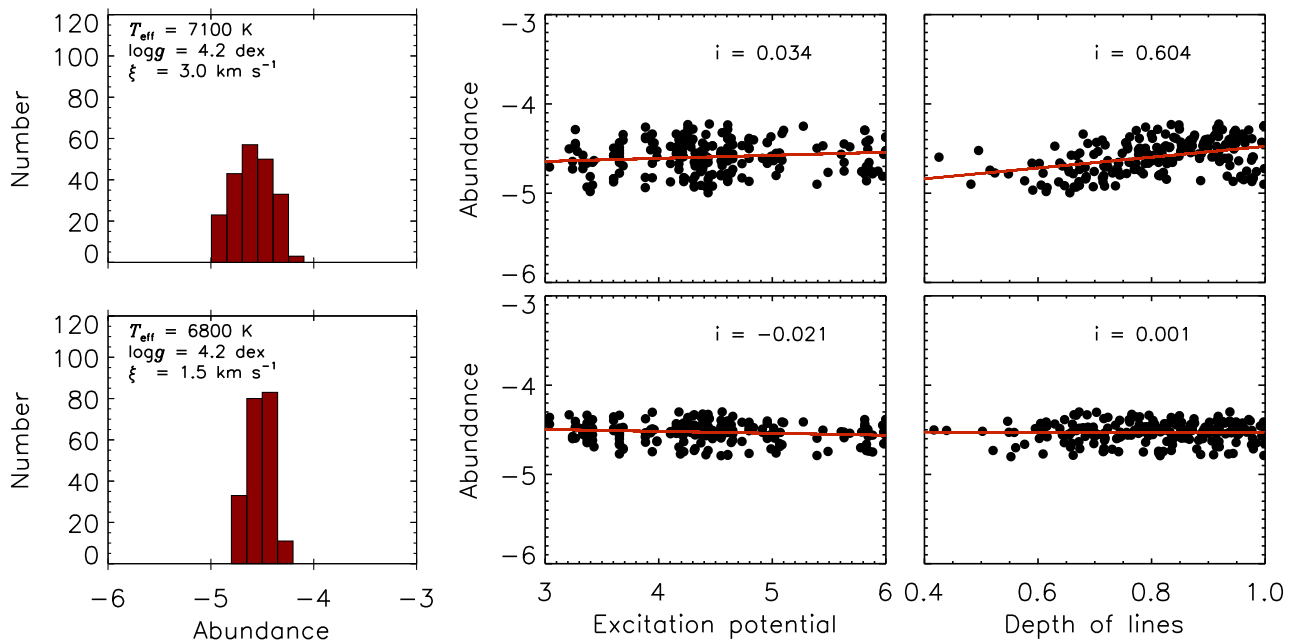


Figure 5. The distributions of the derived iron abundances, the FeI abundances versus the excitation potential and the lines' depths for HD 126516. The 'i' values illustrate an inclination of the fitted line. The first set of parameters ($T_{\text{eff}} = 7100$ K, $\log g = 4.2$ dex, $\xi = 3.0$ km s $^{-1}$) is incorrect (upper panels), while the second set (6800 K, 4.2 dex, 1.5 km s $^{-1}$) is the right one (lower panels).

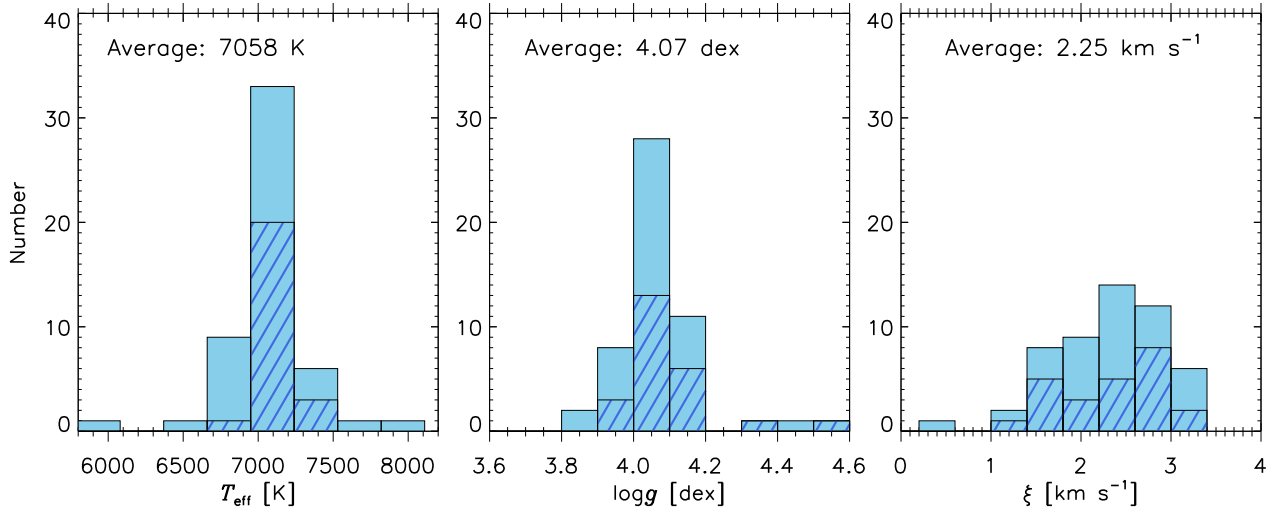


Figure 6. The atmospheric parameters distribution of γ Dor stars. Light blue histograms show the distributions for the full sample while the histograms of the dark blue slant lines illustrates *bona-fide* γ Dor stars.

local thermodynamical equilibrium, plane-parallel geometry, and hydrostatic equilibrium were adopted in calculations of atmospheric models and synthetic spectra. They introduce the error of about 0.1 dex for calculated chemical abundances (Mashonkina 2011). Other important factors are used atomic data, analysed wavelength range, quality of the data (resolution, S/N), and normalisation of the spectra.

To find out the effect of resolution and S/N ratio on the values of the obtained chemical abundances, we selected three stars observed by different instruments with different or similar S/N ratios. First of these stars (HD 109799)

was observed by FIES (R = 67000) and HARPS (R = 80000) spectrographs. Obtained spectra have almost the same S/N ratios (~ 310). We performed the standard analysis of both spectra and obtained a 0.07 dex difference in iron abundance. For the second star (HD 23005) the spectra were collected by FIES (R = 67000) with S/N = 300 and by HERMES (R = 85000) with S/N = 180 ratio. According to the S/N ratio and the resolving power of these spectra, both spectra have approximately the same quality. In case of this star, we got the difference in iron abundance of about 0.02 dex. For the third star (HD 133803) we have spectra

from HARPS ($R=80000$) with $S/N=310$ ratio and from HERMES ($R=85000$) with $S/N=170$ ratio. The spectra have nearly the same resolution but different S/N values. When we compared the obtained abundances of iron, 0.13 dex difference was derived. These calculations show, that the resolving power does not have significant influence on abundance determinations in our spectral analysis, as all data were taken by high-resolution instruments. On the other hand, the S/N ratio has more important effect.

We also checked the possible influence of quality of the spectrum on atmospheric parameters determination. The stars were observed by spectrographs with resolving powers equal 67000, 80000 and 85000. Collected spectra have S/N more than 100, often S/N more than 150. We can state that the latter value is the recommended one to be used in the abundance analyses, since the improvements obtained with higher S/N spectra could not be justified by larger investment of observing time. However, we found no substantial effect of the resolving power and S/N ratio on atmospheric parameters. Similar results were also obtained by Ryabchikova et al. (2015).

The influence of uncertainties of atmospheric parameters and $v \sin i$ on chemical abundances was examined as well. We obtained that 100 K uncertainty of T_{eff} causes the change in element abundance of less than 0.1 dex. This value increases with increasing T_{eff} . On the other hand, the 0.1 dex error of $\log g$ changes the chemical abundances of about 0.04 dex or less. Additionally, we found that for stars in our effective temperature range, 0.1 km s^{-1} uncertainty in ξ value changes the element abundance of less than 0.1 dex. The significant influence on the determined abundances can obtain the uncertainty of the $v \sin i$ value. To examine this effect, we checked the abundance differences caused by changes of $v \sin i$ in the range from ~ 5 to 15 km s^{-1} , depending on the projected rotation velocity of the star. Higher value of $v \sin i$ implies higher value of its uncertainty. These uncertainties cause differences in abundances ranging from 0.1 to 0.2 dex. The effect increases with increasing projected rotational velocity. Finally, we considered all mentioned uncertainties to calculate the total error of chemical abundances. This value can be as high as 0.28 dex but for most cases it is about 0.20 dex. These errors were also calculated by Niemczura et al. (2015) for hotter stars. They found these values less than 0.20 dex for their targets. The total errors of iron abundances are given in Table 4.

5.4 Discussion of the results

Effective temperatures

The stellar T_{eff} parameters were determined by various methods. The final values were obtained from the iron lines analysis. As can be seen in the left-hand panel of Fig. 6, the T_{eff} range for the full sample is between 6000 and 7900 K, while *bona-fide* γ Dor stars have effective temperatures from 7100 to 7300 K. This range is in agreement with the results of the previous studies (Handler & Shobbrook 2002; Bruntt, De Cat, & Aerts 2008; Tkachenko et al. 2012, 2013 a; Van Reeth et al. 2015).

For 12 stars in our survey, the spectroscopic T_{eff} values were determined previously. Information about these stars is given in Table 4. We compared our T_{eff} values with the ones

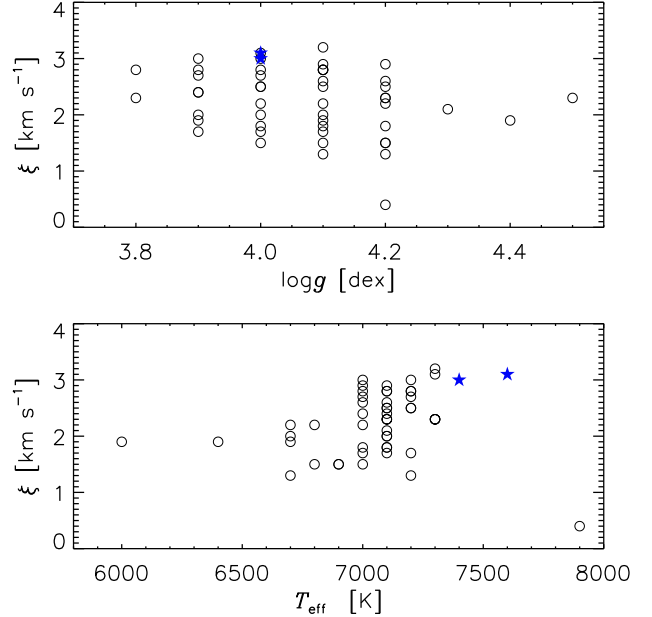


Figure 7. The microturbulent velocities as a function of $\log g$ and T_{eff} . The star symbols represent Am stars HD 33204 and HD 46304.

given in the literature for these objects. It turned out that effective temperatures of the mentioned stars are in agreement within an error of 200 K. Only in the case of HD 46304, the difference between T_{eff} obtained here and that given by Muñoz Bermejo, Asensio Ramos, & Allende Prieto (2013) reaches 400 K. This difference can be explained by the effect of stellar membership in the visual binary system and differences in methods of an atmospheric parameter analysis.

Surface gravities

The $\log g$ values were determined from the analysis of the Fe I and Fe II lines (see Table 4). The distribution of the obtained $\log g$ values is given in the middle panel of Fig. 6. We derived surface gravities between 3.8 and 4.5 dex. Bruntt, De Cat, & Aerts (2008) obtained a $\log g$ range from 3.1 to 4.7 for *bona-fide* and candidate γ Dor stars while Van Reeth et al. (2015) found values between 3.3 and 4.5 for a sample of *bona-fide* γ Dor stars only. In our study, the average $\log g$ value amounts to 4.07 dex for the full sample and the average of 4.09 and 4.05 dex was found for *bona-fide* and candidate γ Dor stars, respectively. These values are slightly lower than those given in previous studies (4.16 dex by Bruntt, De Cat, & Aerts (2008); 4.10 dex by Van Reeth et al. (2015)) what indicates that the stars analysed here are more evolved. From a comparison of our $\log g$ values with those found in the literature, we conclude that they agree within 0.2 dex.

Microturbulent velocities

The obtained microturbulent velocities range from 1.3 to 3.2 km s^{-1} (see right-hand panel of Fig. 6) for all stars except for HD 75202. This star is a candidate

γ Dor star, listed in a catalogue of contact binary objects (Pribulla, Kreiner, & Tremko 2003). The spectrum of HD 75202 can be affected by the other system member, which can influence the determined atmospheric parameters.

The range of ξ values is in agreement with the results of Landstreet et al. (2009), Gebran et al. (2014), and Niemczura et al. (2015). According to these studies, for effective temperatures between 7000 and 8000 K ξ values are mostly between 2 and 4 km s^{-1} . The value of this parameter decreases for temperatures lower than ~ 7000 K and higher than ~ 8000 K. In the case of chemically peculiar Am stars, the ξ values are expected to be higher than for normal stars (Landstreet et al. 2009). We plotted the ξ parameter as a function of T_{eff} in the right-hand panel of Fig. 7. As can be seen, the Am stars in our study show the same ξ values as non-chemically peculiar stars. A similar result for Am stars was obtained by Niemczura et al. (2015) and Smalley (2004). We also examined the variation of ξ values with surface gravity (left-hand panel of Fig. 7). The ξ values are lower with increasing values of $\log g$. The same variations for F type stars were obtained by Gray, Graham, & Hoyt (2001).

Van Reeth et al. (2015) found ξ values between 2 and 3.5 km s^{-1} for γ Dor stars, in agreement with our results. The small differences are due to the differences in the applied methods and adopted atomic data.

Projected rotational velocities

The $v \sin i$ values were derived during the analysis of the chemical abundances by the spectrum synthesis method. The range of the obtained projected rotational velocities is between 5 and 240 km s^{-1} . The distribution of $v \sin i$ is shown in Fig. 8. The average $v \sin i$ value equal to 80 km s^{-1} was calculated taking into account all analysed stars. When considering *bona-fide* and candidate γ Dor stars separately, the average values are 97 and 63 km s^{-1} , respectively. In the previous studies, this value obtained for *bona-fide* and candidate γ Dor stars equals 57 km s^{-1} (Henry & Fekel 2002, 2003; Fekel, Warner, & Kaye 2003; Mathias et al. 2004; De Cat et al. 2006; Van Reeth et al. 2015). Van Reeth et al. (2015) gives the range from 12 to 204 km s^{-1} and the average value of 71 km s^{-1} for *bona-fide* γ Dor stars. All these values depend on the analysed sample of stars. However, both our results and Van Reeth et al. (2015) calculations suggest a great variation of projected rotational velocities of *bona-fide* γ Dor stars.

In our study, most stars have high projected rotational velocities ($v \sin i > 100 \text{ km s}^{-1}$). However, during the analysis we found some slowly rotating stars (HD 21788, HD 104860, HD 109838 and HD 126516) with $v \sin i < 15 \text{ km s}^{-1}$. Not all chemically peculiar stars from our sample are slowly rotating stars. HD 33204 has $v \sin i$ value of 36 km s^{-1} while HD 46304 has $v \sin i = 242 \text{ km s}^{-1}$. It has been shown that Am stars generally have smaller rotational velocities than normal stars (Abt & Hudson 1971).

Chemical abundances

The abundance pattern of γ Dor stars was examined in detail. The average relative abundance of *bona-fide*, candi-

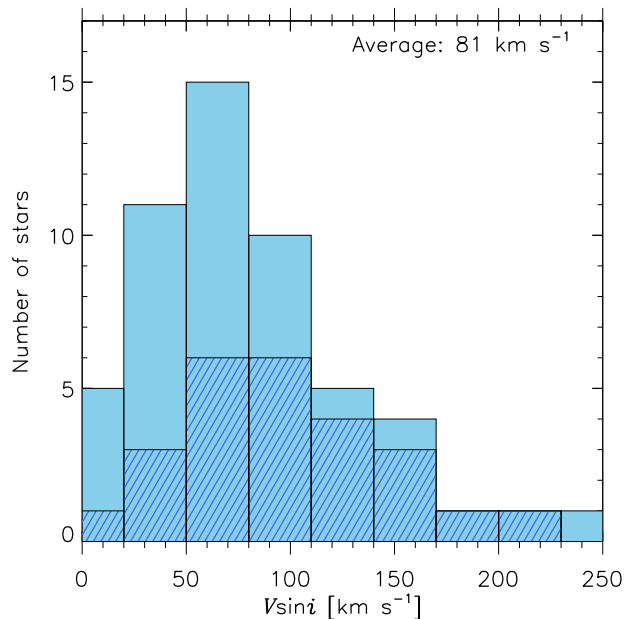


Figure 8. The rotational velocity distribution of the stars. The light blue histogram shows the distribution for full sample while the histogram of dark blue slant lines illustrates the distribution *bona-fide* γ Dor stars.

date γ Dor, and non-pulsating F type stars were compared. The abundance distributions of four non-pulsating F type stars were taken from Niemczura et al. (2015), as the same analysis method is used in the current study. This comparison is demonstrated in Fig. 9. As can be seen, the abundances of both *bona-fide* and candidate γ Dor stars are close to the solar abundances.

The abundances of Am: stars were also examined in detail. As mentioned before, we identified two mild-Am stars, HD 33204 and HD 46304. We show abundance distributions of these stars in Fig. 10. A typical Am star exhibits overabundances of iron-peak elements and some heavy elements (Zn, Sr, Zr and Ba), but Ca and Sc abundances of these stars are underabundant (Gray & Corbally 2009). As can be seen in Fig. 10, the mild-Am stars in our study have nearly solar abundances of Ca and Sc elements. Only HD 33204 shows overabundances in some heavy elements typical for Am star. In the case of HD 46304, most of lines are blended due to high rotation velocity of the star. These blended lines cause difficulties in abundance calculations. The abundance differences between HD 46304 and a typical Am star can be caused by this effect. In the spectral classification process some stars were defined as metal-poor, mostly taking into account Mg, Mn and Fe lines (see Table 2). For these stars, the average abundance of Mg (7.57 dex) was found to be close to the solar abundance. However, the average abundances of Mn (5.13 dex) and Fe (7.27 dex) are slightly lower than the solar abundances. For some of our targets (HD 26298, HD 33204, HD 106103, HD 110379, and HD 126516) chemical abundances were already obtained before the present study. We compared our atmospheric parameters and abundance results with the literature values. Abundances of HD 33204 and HD 10613 were derived by Varenne & Monier (1999) and Fossati et al. (2008), respectively. In their work, sim-

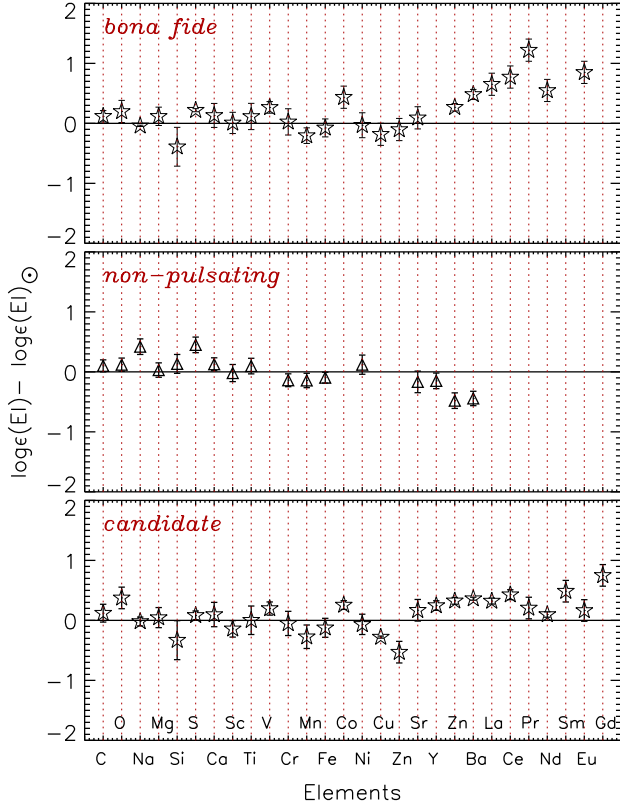


Figure 9. Chemical abundances of the *bona-fide*, candidate γ Dor stars and the non-pulsating F type stars. Solar abundances and those of non-pulsating stars were taken from Asplund et al. (2009) and Niemczura et al. (2015), respectively.

ilar methods for abundance analysis were used but different atomic data bases were adopted. For HD 33204 higher abundances of Sc, Mg and Y were obtained in the present study. Our result is consistent with the Am: type peculiarity of this star. For HD 106103 only the Y abundance is different. Abundances of HD 26298, HD 110379 and HD 126516 were derived by Bruntt, De Cat, & Aerts (2008) using the equivalent width method and the different atomic data base. In the case of these three stars, the marked differences were detected only for V and Ba abundances.

Additionally, we checked the possible correlations of the element abundances with atmospheric parameters, i.e. T_{eff} , $\log g$ and ξ . Similar as in Niemczura et al. (2015), no correlations were found. Moreover, the element abundances do not depend on $v \sin i$. The same result was found by Fossati et al. (2008). However, Takeda et al. (2008) reported negative correlations between $v \sin i$ and C, O and Ca elements. Finally, we checked the relations between abundances of iron and other elements. Strong positive correlations were found for Mg, Si, Ca, Sc, Ti Cr, Ni, Y and Ba. Similar correlations between Fe abundances and iron-peak elements were found by Niemczura et al. (2015). On the other hand, a negative correlation was obtained between Fe and O abundances.

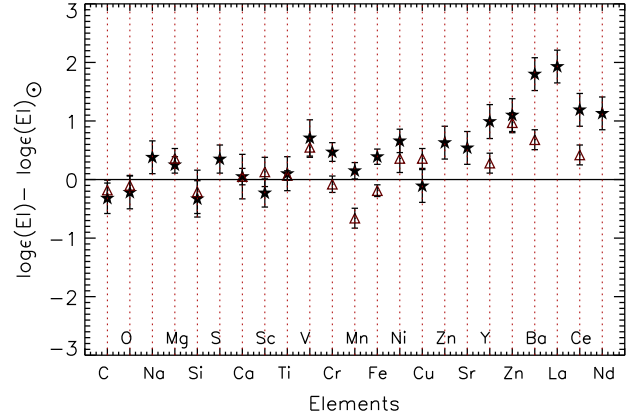


Figure 10. Chemical abundances of Am: stars compared with the solar values (Asplund et al. 2009). HD 33204 is represented by stars and HD 46304 by triangles.

6 DISCUSSION AND CONCLUSIONS

This study presents a detailed analysis of the atmospheric parameters and chemical abundances of a sample *bona-fide* and candidate γ Dor stars. We analysed the high-resolution and high S/N spectra of 52 objects. The results of the spectral classifications show that the spectral types of γ Dor stars are between A7 and F9 and that their luminosity classes range from V to IV. During the spectral classifications process, two mild-Am stars, HD 33204 and HD 46304 were defined. Peculiarities of these stars were checked with the results of the detailed abundance analysis. Only for HD 33204 this peculiarity was confirmed. Because of the high rotation velocity of HD 46304, the peculiarity of this star could not be confirmed.

To determine the initial atmospheric parameters (T_{eff} and $\log g$), we used photometric indices, SEDs and hydrogen lines. The obtained T_{eff} values were compared with each other. We found that effective temperatures from different methods are mostly in agreement. The final atmospheric parameters of the stars were derived from iron lines analysis using the spectrum synthesis method. The agreement between the new results obtained with our analysis and those previously available shows the robustness of the spectroscopic procedures adopted to analyse the chemical abundances of A-F stars.

For the whole sample, the obtained T_{eff} values range from 6000 to 7900 K, while the obtained $\log g$ changes from 3.8 to 4.5 dex. This result corresponds with the obtained luminosity type of the stars. Additionally, the ξ parameters were derived in the range of 1.3–3.2 km s^{-1} . The stars in our sample have mostly moderate and high rotation velocities. The obtained $v \sin i$ values are between 5 and 240 km s^{-1} , while average values are equal to 97 and 63 km s^{-1} for the *bona-fide* and the candidate stars, respectively.

After the determination of accurate stellar parameters, relations between T_{eff} , $\log g$, ξ and $v \sin i$ and pulsation periods and V-band amplitudes of the γ Dor stars were investigated. The stellar pulsation parameters were taken from the papers given in Table 2. The existence of the correlation between the pulsation and rotation periods of variables was suggested by Balona et al. (2011). Also we found a strong

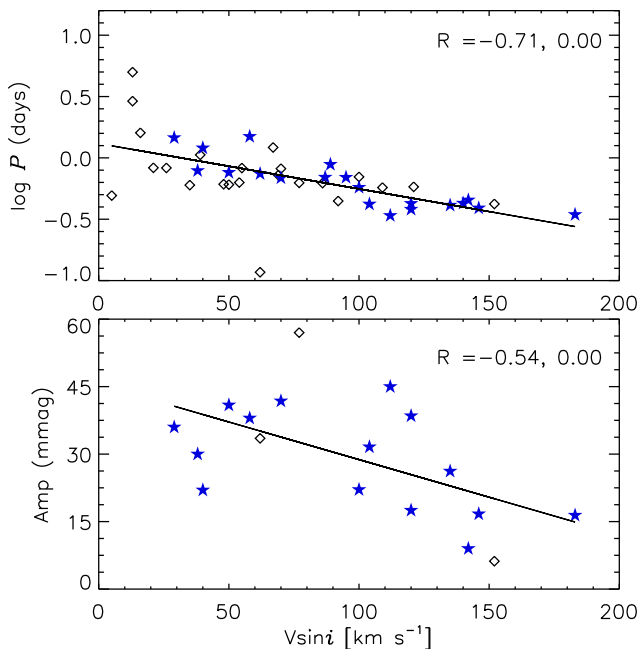


Figure 11. The comparison of $v \sin i$ with the pulsation period and amplitude of γ Dor stars. *Bona-fide* and candidate γ Dor variables are represented by stars and diamonds, respectively. The first number of R constant shows strength of the correlation (in the ideal case close to 1) while the second number represents deviations of points from the correlations (in the ideal case close to 0).

relation between $v \sin i$ parameter and pulsation period, as shown in Fig. 11. The similar result was obtained in the previous studies (e.g. Tkachenko et al. 2013 b; Van Reeth et al. 2015). This shows that the pulsation periods of stars decrease with increasing $v \sin i$ values. This result is in agreement with the theoretical study of Bouabid et al. (2013), where it was shown that g-mode frequencies are shifted to higher frequencies by rotation. On the other hand, we could not find a clear correlation between pulsation period and T_{eff} values, despite the positive relation found by Van Reeth et al. (2015). We also found weak correlations between the pulsation amplitude and both $\log g$ values and relative iron abundances. Additionally, the correlation between pulsation periods and ξ was obtained. These correlations are presented in Fig. 12. As can be seen from this figure, more data is necessary in order to establish the exact relations between those parameters.

The comprehensive abundance analysis of both *bona-fide* and candidate γ Dor stars was performed using the spectrum synthesis method. We compared chemical abundances of *bona-fide* γ Dor stars with those obtained for candidates and F type non-pulsating stars. According to these comparisons, no obvious differences were obtained. These stars have abundances close to the solar values (Asplund et al. 2009). The derived average iron abundances are equal 7.42 and 7.38 dex for *bona-fide* and candidate γ Dor stars, respectively. These values are also close to the solar iron abundances (7.50 dex).

In Fig. 13, the positions of the studied stars in the theoretical instability strips of γ Dor and δ Sct stars are given. The evolutionary tracks shown in this figure were calculated

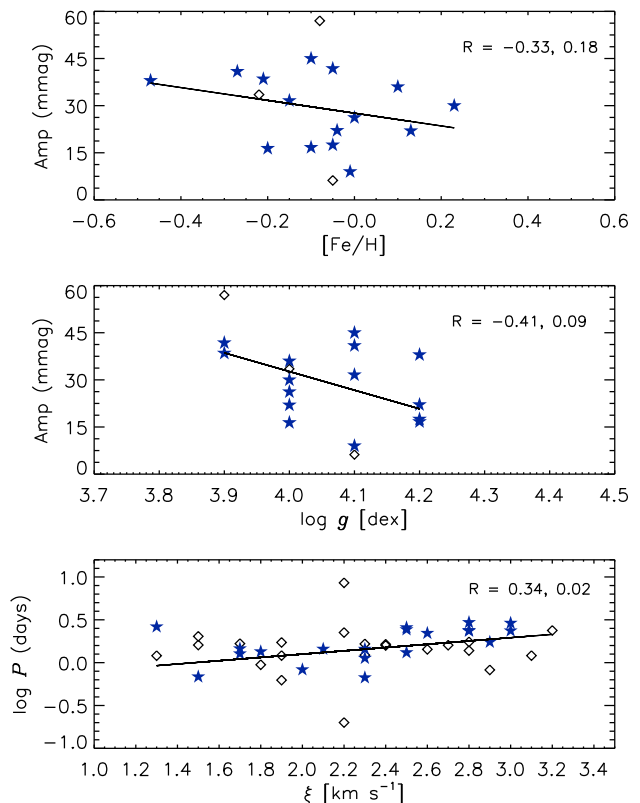


Figure 12. The relations between the pulsation period and pulsation amplitude of γ Dor stars and certain parameters given in x-axis. Stars and diamonds represent *bona-fide* and candidate γ Dor variables, respectively. The R constant has the same meaning as in Fig. 11.

with the MESA (Modules for Experiments in Stellar Astrophysics) evolution code (Paxton et al. 2011, 2013, 2015). All the computed models have an initial hydrogen abundance of $X = 0.7$, the initial helium abundance of $Y = 0.28$ and use the AGSS09 metal mixture (Asplund et al. 2009). The initial metal abundance is $Z = 0.02$. The OPAL (Iglesias & Rogers 1996) opacity tables were used. All effects of rotation were neglected. The convective zones were determined by the Ledoux criterion. For the envelope, we adopted the parameter of the mixing length theory (MLT) of $\alpha_{\text{mit}} = 2.0$, as the theoretical instability strip of γ Dor stars were calculated with this value by Dupret et al. (2005).

The positions of γ Dor stars in both theoretical instability strips have been discussed in the literature. In Uytterhoeven et al. (2011), γ Dor stars were mostly found outside their theoretical instability strip. The same result was also presented in Grigahcène et al. (2010) and Tkachenko et al. (2012, 2013 a), whereas Tkachenko et al. (2013 b) found them inside the γ Dor instability strip within errors. As can be seen in Fig. 13, *bona-fide* γ Dor stars mostly cluster at the blue edge of the γ Dor instability strip, while some of them are located in δ Sct domain. Only HD 104860 is located outside those instability strips. Considering the received atmospheric parameters of this star, we conclude that HD 104860 is not a γ Dor variable.

In this study, we obtained accurate atmospheric param-

eters and chemical composition of a large sample of the γ Dor stars. They are essential in modelling of the pulsation and in the understanding of the real evolutionary status and stellar structure. As a result, we found that our stars are mostly located close to the blue edge of the γ Dor instability strip, where δ Sct pulsation (i.e., pressure modes) is also possible. This seems reduce a little the range of the γ Dor pulsation in the classical instability strip described by Uytterhoeven et al. (2011). In the follow-up paper, we plan to perform a detailed spectroscopic study of SB2 γ Dor stars. The investigation of the sample of SB2 stars will give us the possibility to examine the probable differences of chemical abundances and atmospheric parameters with respect to the single stars studied in this paper.

ACKNOWLEDGEMENTS

The authors would like to thank the reviewer for useful comments and suggestions that helped to improve the publication. This work has been partly supported by the Scientific and Technological Research Council of Turkey (TUBITAK) grant numbers 2214-A and 2211-C. This article is a part of the Ph.D. thesis of FKA. FKA wishes to express gratitude to professor Dr J. A. Guzik for all assistance given at the start of this project. EN acknowledges support from the NCN grant No. 2014/13/B/ST9/00902. The calculations have been carried out in Wrocław Centre for Networking and Supercomputing (<http://www.wcss.pl>), grant No. 214. We thank professor Dr R. O. Gray and Dr. B. Smalley for their helpful comments. We are grateful to Dr. D. Shulyak for putting the code for calculating SEDs at our disposal. We thank to Dr. G. Catanzaro for putting the code for Balmer lines analysis at our disposal. “Ministerio de Economía y Competitividad” (MINECO) and FEDER funds under the “Ramón y Cajal” subprogram, also acknowledges support by the European project SpaceInn (ref. 312844) within the European SPACE program FP7-SPACE-2011-1, and from Junta de Andalucía (Spanish) local government under project Contribución Andaluza al proyecto espacial CoRoT with reference P12-TIC-2469. This work is partially based on observations collected at La Silla Observatory, ESO (Chile) with the FEROS and HARPS spectrographs under programmes LP178.D-0361, LP182.D-0356, and LP185.D-0056. EP and MR acknowledge financial support from the FP7 project “SpaceInn: Exploitation of Space Data for Innovative Helio and Asteroseismology” from PRIN-INAF 2014 *Galactic Archaeology*. This research has made use of the SIMBAD data base, operated at CDS, Strasbourg, France.

REFERENCES

- Abt H. A., Hudson K. I., 1971, *ApJ*, 163, 333
 Adelman S. J., Pyper D. M., Shore S. N., White R. E., Warren W. H., Jr., 1989, *A&AS*, 81, 221
 Aerts C., Eyer L., Kestens E., 1998, *A&A*, 337, 790
 Alekseeva G. A., et al., 1996, *BaltA*, 5, 603
 Ammler-von Eiff M., Reiners A., 2012, *A&A*, 542, A116
 Amôres E. B., Lépine J. R. D., 2005, *AJ*, 130, 659
 Asplund M., Grevesse N., Sauval A. J., Scott P., 2009, *ARA&A*, 47, 481
 Balona L. A., Krisciunas K., Cousins A. W. J., 1994, *MNRAS*, 270, 905
 Balona L. A., Guzik J. A., Uytterhoeven K., Smith J. C., Tenenbaum P., Twicken J. D., 2011, *MNRAS*, 415, 3531
 Borucki W. J., et al., 2010, *Sci*, 327, 977
 Boksenberg A., et al., 1973, *MNRAS*, 163, 291
 Bouabid M.-P., Dupret M.-A., Salmon S., Montalbán J., Miglio A., Noels A., 2013, *MNRAS*, 429, 2500
 Breger M., 1976, *ApJS*, 32, 7
 Bruntt H., De Cat P., Aerts C., 2008, *A&A*, 478, 487
 Burnashev V. I., 1985, *A&OB*, 59, 83
 Catanzaro G., Leone F., Dall T. H., 2004, *A&A*, 425, 641
 Cousins A. W. J., 1992, *Obs*, 112, 53
 Cutri R. M., et al., 2003, 2MASS All Sky Catalog of point sources.
 De Cat P., et al., 2006, *A&A*, 449, 281
 Dubath P., et al., 2011, *MNRAS*, 414, 2602
 Dupret M.-A., Grigahcène A., Garrido R., Gabriel M., Scuflaire R., 2004, *A&A*, 414, L17
 Dupret M.-A., Grigahcène A., Garrido R., Gabriel M., Scuflaire R., 2005, *A&A*, 435, 927
 Elkin V. G., Kurtz D. W., Nitschelm C., 2012, *MNRAS*, 420, 2727
 Eyer L. PhD Thesis, 1998
 Fekel F. C., Warner P. B., Kaye A. B., 2003, *AJ*, 125, 2196
 Fossati L., Bagnulo S., Landstreet J., Wade G., Kochukhov O., Monier R., Weiss W., Gebran M., 2008, *A&A*, 483, 891
 Gebran M., Monier R., Royer F., Lobel A., Blomme R., 2014, *psce.conf*, 193
 Glushneva I. N., Kharitonov A. V., Kniazeva L. N., Shenavrin V. I., 1992, *A&AS*, 92, 1
 Gray R. O., Garrison R. F., 1989, *ApJS*, 70, 623
 Gray R. O., Graham P. W., Hoyt S. R., 2001, *AJ*, 121, 2159
 Gray R. O., Corbally C. J., Garrison R. F., McFadden M. T., Robinson P. E., 2003, *AJ*, 126, 2048
 Gray R. O., Corbally C., J., 2009, *Stellar Spectral Classification*, Princeton University Press
 Grigahcène A., et al., 2010, *ApJ*, 713, L192
 Guzik J. A., Kaye A. B., Bradley P. A., Cox A. N., Neuforge C., 2000, *ApJ*, 542, L57
 Handler G., 1999, *MNRAS*, 309, L19
 Handler G., Shobbrook R. R., 2002, *MNRAS*, 333, 251
 Hareter M., Fossati L., Weiss W., Suárez J. C., Uytterhoeven K., Rainer M., Poretti E., 2011, *ApJ*, 743, 153
 Hearnshaw J. B., Barnes S. I., Frost N., Kershaw G. M., Graham G., Nankivell G. R., 2003, *ASPC*, 289, 11
 Henry G. W., Fekel F. C., Kaye A. B., Kaul A., 2001, *AJ*, 122, 3383
 Henry G. W., Fekel F. C., 2002, *PASP*, 114, 999
 Henry G. W., Fekel F. C., 2003, *AJ*, 126, 3058
 Henry G. W., Fekel F. C., 2005, *AJ*, 129, 2026
 Henry G. W., Fekel F. C., Henry S. M., 2007, *AJ*, 133, 1421
 Henry G. W., Fekel F. C., Henry S. M., 2011, *AJ*, 142, 39
 Iglesias C. A., Rogers F. J., 1996, *ApJ*, 464, 943
 Kaye A. B., Handler G., Krisciunas K., Poretti E., Zerbi F. M., 1999, *PASP*, 111, 840
 Kharchenko N. V., Piskunov A. E., Röser S., Schilbach E., Scholz R.-D., 2005, *A&A*, 438, 1163
 King J. R., Schuler S. C., 2005, *PASP*, 117, 911
 Krisciunas K., et al., 1993, *MNRAS*, 263, 781
 Krisciunas K., Handler G., 1995, *IBVS*, 4195, 1

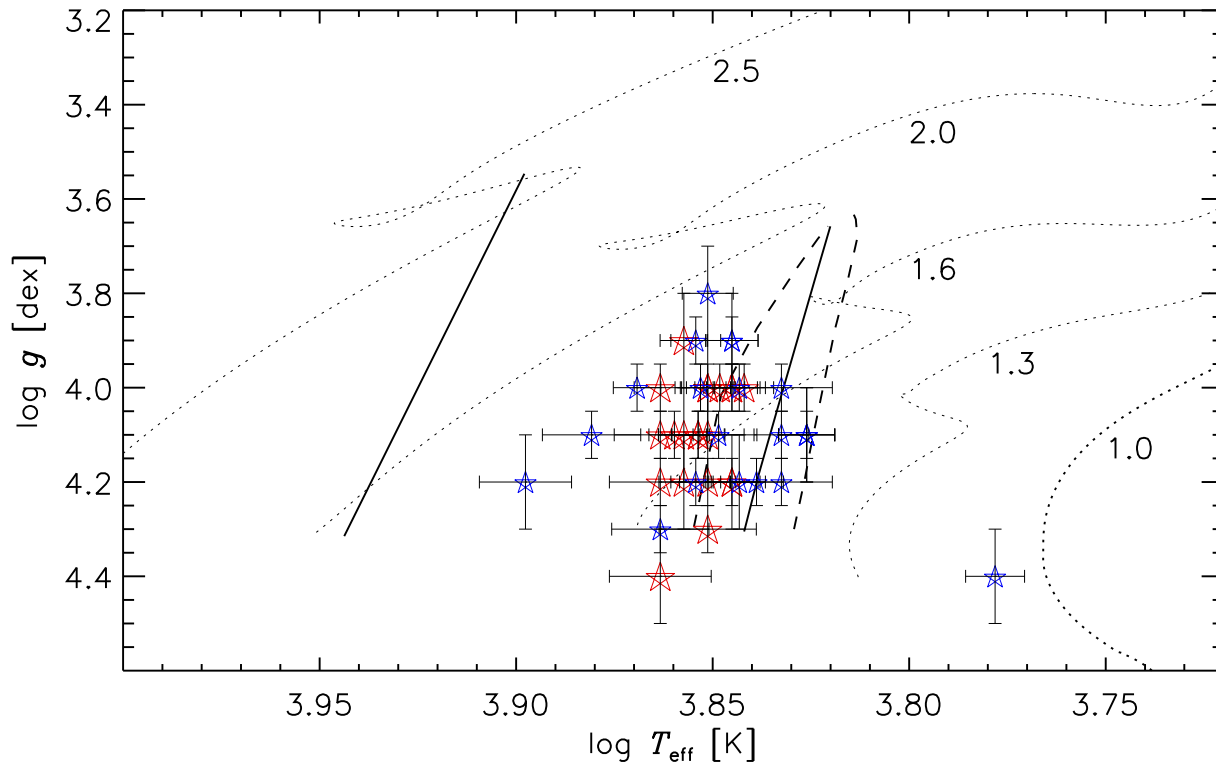


Figure 13. Positions of the *bona-fide* (bigger red stars) and candidate (small blue stars) γ Dor stars in the theoretical instability strips of the γ Dor (dashed-lines) and δ Sct (solid lines) stars (Dupret et al. 2005).

Künzli M., North P., Kurucz R. L., Nicolet B., 1997, *A&AS*, 122, 51
 Kurtz D. W., Saio H., Takata M., Shibahashi H., Murphy S. J., Sekii T., 2014, *MNRAS*, 444, 102
 Kurucz R. L., Avrett E. H., 1981, *SAOSR*, 391,
 Kurucz R., 1993, *KurCD*, 13,
 Kurucz R., Bell B., 1995, *KurCD*, 23,
 Landstreet J. D., Kupka F., Ford H. A., Officer T., Sigut T. A. A., Silaj J., Strasser S., Townshend A., 2009, *A&A*, 503, 973
 Martín S., Rodríguez E., 2000, *A&A*, 358, 287
 Masana E., Jordi C., Ribas I., 2006, *A&A*, 450, 735
 Mashonkina L., 2011, *mast.conf*, 314
 Mathias P., et al., *Proc. 4th COROT week*, Marseille, 26 June.
 Mathias P., et al., 2004, *A&A*, 417, 189
 Mayor M., et al., 2003, *Msngr*, 114, 20
 Mermilliod J.-C., Mermilliod M., Hauck B., 1997, *A&AS*, 124, 349
 Miglio A., Montalbán J., Noels A., Eggenberger P., 2008, *MNRAS*, 386, 1487
 Moon T. T., Dworetzky M. M., 1985, *MNRAS*, 217, 305
 Munari U., Zwitter T., 1997, *A&A*, 318, 269
 Muñoz Bermejo J., Asensio Ramos A., Allende Prieto C., 2013, *A&A*, 553, A95
 Niemczura E., Smalley B., Pych W., 2014, *Determination of Atmospheric Parameters of B-, A-, F- and G-Type Stars Lectures from the School of Spectroscopic Data Analyses*
 Niemczura E., et al., 2015, *MNRAS*, 450, 2764
 Raskin G., et al., 2011, *A&A*, 526, A69
 Ryabchikova T., et al., 2015, *arXiv*, arXiv:1511.06134

Paxton B., Bildsten L., Dotter A., Herwig F., Lesaffre P., Timmes F., 2011, *ApJS*, 192, 3
 Paxton B., et al., 2013, *ApJS*, 208, 4
 Paxton B., et al., 2015, *arXiv*, arXiv:1506.03146
 Pribulla T., Kreiner J. M., Tremko J., 2003, *CoSka*, 33, 38
 Poretti E., et al., 2003, *A&A*, 406, 203
 Saio H., Kurtz D. W., Takata M., Shibahashi H., Murphy S. J., Sekii T., Bedding T. R., 2015, *MNRAS*, 447, 3264
 Sekiguchi M., Fukugita M., 2000, *AJ*, 120, 1072
 Smalley B., Gardiner R. B., Kupka F., Bessell M. S., 2002, *A&A*, 395, 601
 Smalley B., 2004, *IAUS*, 224, 131
 Smalley B., 2005, *MSAIS*, 8, 130
 Takeda Y., Han I., Kang D.-I., Lee B.-C., Kim K.-M., 2008, *JKAS*, 41, 83
 Telting J. H., et al., 2014, *AN*, 335, 41
 Thompson G. I., Nandy K., Jamar C., Monfils A., Houzi-iaux L., Carnochan D. J., Wilson R., 1978, *csuf.book*,
 Tkachenko A., Lehmann H., Smalley B., Deboscher J., Aerts C., 2012, *MNRAS*, 422, 2960
 Tkachenko A., Lehmann H., Smalley B., Uytterhoeven K., 2013 a, *MNRAS*, 431, 3685
 Tkachenko A., et al., 2013 b, *A&A*, 556, A52
 Uytterhoeven K., Moya, A., Grigahcène A., Guzik, J. A., Gutiérrez-Soto, J., et al., 2011, *A&A*, 534, AA125
 Uytterhoeven K., et al., 2011, *arXiv*, arXiv:1111.1840
 van Leeuwen F., 2007, *A&A*, 474, 653
 Van Reeth T., et al., 2015, *ApJS*, 218, 27
 Varenne O., Monier R., 1999, *A&A*, 351, 247
 Wamsteker W., Skillen I., Ponz J. D., de la Fuente A., Barylak M., Yurrita I., 2000, *Ap&SS*, 273, 155

Wenger M., et al., 2000, A&AS, 143, 9

Woodgate B. E., et al., 1998, PASP, 110, 1183

Table 2. Spectroscopic observations and the spectral classification of the investigated stars.

HD number	Instruments	Number of spectra	V (mag)	Sp type (Simbad)	Sp type (this study)	Notes	References
009365**	FIES	1	8.23	F0	F1 V	γ Dor	1
019655	FIES	3	8.62	F2 V	F1 V nn	γ Dor	3
021788	FIES	2	7.50	F0	F3 V	cand γ Dor	2
022702	FIES	3	8.80	A2	F1 IV	γ Dor	3
023005	FIES	4	5.82	F0 IV	F1 IV nn	cand γ Dor	2
023585	FIES	1	8.36	F0 V	F0 V	γ Dor	3
026298**	FIES	1	8.16	F1 V	F2 V	cand γ Dor	4
033204	FIES	1	6.01	A5 m	A7 V Am:	cand γ Dor	5
046304	FIES	3	5.60	F0 V	A8 V Am:	cand γ Dor	16
063436	FIES	1	7.46	F2	F0 IV	γ Dor	6
089781	FIES	1	7.48	F0	F1 V	γ Dor	1
099267	FIES	3	6.87	F0	F1 V	γ Dor	6
099329	FIES	3	6.37	F3 IV	F2 IV nn	γ Dor	1
104860	FIES	2	7.91	F8	G0 / F9 V	cand γ Dor	2
106103	FIES	1	8.12	F5 V	F2 - 3 V	cand γ Dor	14
107192	FIES	1	6.28	F2 V	F1 IV	cand γ Dor	7
109032	FIES	5	8.09	F0	F1 V	cand γ Dor	2
109799	FIES	1	5.45	F1 IV	F2 IV	cand γ Dor	2
109838	FIES	1	8.04	F2 V	F2 IV	cand γ Dor	2
110379	FIES	1	3.44	F0 IV	F1 - F2 V	cand γ Dor	4
112429	FIES	1	5.24	F0 IV-V	F3 IV	γ Dor	6
118388	FIES	3	7.98	F2	F5 V m - 3	cand γ Dor	8
126516**	FIES	2	8.31	F3 V	F5 V	cand γ Dor	4
130173**	FIES	1	6.88	F3 V	F5 V m - 3	cand γ Dor	9
155154	FIES	3	6.18	F0 IV-Vn	F2 IV nn	γ Dor	10
165645	FIES	3	6.36	F0 V	F1 V nn	cand γ Dor	6
169577	FIES	5	8.65	F0	F1 V	γ Dor	11
187353	FIES	3	7.55	F0	F1 IV/V	cand γ Dor	2
206043	FIES	1	5.87	F2 V	F1 V nn	γ Dor	10
075202	HARPS	5	7.75	A3 IV	A7 V	cand γ Dor	8
091201	HARPS	5	8.12	F1 V/IV	F1 V / IV	cand γ Dor	2
103257	HARPS	5	6.62	F2 V	F2 V m - 2	cand γ Dor	2
113357	HARPS	14	7.87	F0 V	F2 V m - 2	cand γ Dor	2
133803	HARPS	4	8.15	A9 V	F2 IV m - 2	cand γ Dor	2
137785	HARPS	6	6.43	F2 V	F2 V	cand γ Dor	2
149989	HARPS	6	6.29	A9 V	F1 V nn m-4	γ Dor	4
188032	HARPS	10	8.14	A9 / F0 V	A9 V	cand γ Dor	2
197451**	HARPS	3	7.18	F1	F0 V	cand γ Dor	2
206481	HARPS	7	7.86	F0 V	F2 V	γ Dor	2
224288	HARPS	5	8.04	F0 V	F2 IV/V	cand γ Dor	2
112934	HERCULES	2	6.57	A9 V	A9 V	cand γ Dor	4
115466	HERCULES	2	6.89	F0	F1 IV/V	γ Dor	12
124248	HERCULES	2	7.17	A8 V	A8 - A7 V	γ Dor	12
171834	HERCULES	4	5.45	F3 V	F3 V	γ Dor	15
172416	HERCULES	23	6.62	F5 V	F6 V	cand γ Dor	2
175337	HERCULES	2	7.36	F5 V	F2 V	γ Dor	12
187028	HERCULES	2	7.60	F0 V	F2 V	γ Dor	4
209295**	HERCULES	2	7.32	A9 / F0 V	A9 / F0 V - IV	γ Dor	4
216910	HERCULES	2	6.69	F2 IV	F2 V	γ Dor	4
224638	HERCULES	2	7.48	F0	F2 - F3 IV	γ Dor	6
224945	HERCULES	1	6.62	A3	A9 V / IV	γ Dor	6
041448	HERMES	1	7.62	A9 V	A9 V	γ Dor	6

References - (1) Henry, Fekel, & Henry (2007); (2) Handler (1999); (3) Martín & Rodríguez (2000); (4) De Cat et al. (2006)

(5) Eyer PhD (1998); (6) Henry, Fekel, & Henry (2011); (7) Aerts, Eyer, & Kestens (1998); (8) Dubath et al. (2011)

(9) Fekel, Warner, & Kaye (2003); (10) Henry et al. (2001); (11) Poretti et al. (2003); (12) Henry & Fekel (2005)

(13) Handler & Shobbrook (2002); (14) Krisciunas & Handler (1995); (15) Uytterhoeven et al. (2011); (16) Mathias et al. (2003)

Notations : IV / V=between IV - V, IV-V= whether IV or V, nn=very rapid rotators, m-* = metallicity class where * represents number, "Am:" defines a mild Am star, cand = candidate, **=SB1 stars.

Table 3. The $E(B - V)$ values and atmospheric parameters derived from the photometric indices and SED analysis.

HD number	$E(B - V)$ <i>Map</i> (mag)	$E(B - V)$ <i>NaD₂</i> (mag)	T_{eff} <i>uvbyβ</i> (K) ± 95	$\log g$ <i>uvbyβ</i> (dex) ± 0.10	T_{eff} <i>Geneva</i> (K) ± 125	$\log g$ <i>Geneva</i> (dex) ± 0.11	T_{eff} <i>UBV</i> (K) ± 170	T_{eff} <i>2MASS</i> (K) ± 80	T_{eff} <i>Average*</i> (K) ± 245	T_{eff} <i>SED</i> (K)
009365	0.01	0.00	7050	4.05			7200	6940	7060	7280 \pm 190
019655	0.03	0.03	6950	3.96	6850	4.06	7110	7130	7010	6800 \pm 150
021788	0.02	0.02	6530	3.46			6930	6680	6750	6860 \pm 200
022702	0.03	0.03			6940	4.28	7050	7040	7010	6800 \pm 100
023005	0.00	0.00	7030	3.88	6920	4.07	6940	6870	6940	6970 \pm 120
023585	0.03	0.00	7530	4.31	7080	4.26	7180	7220	7250	6990 \pm 170
026298	0.01	0.00	6730	4.11	6720	4.38	6910	6820	6790	6670 \pm 130
033204	0.00	0.00	7650	4.11	7210	4.04	7330	7510	7425	7170 \pm 150
046304	0.00	0.00	7380	3.88	7370	4.25	7430	7270	7360	7150 \pm 150
063436	0.00	0.00	7350	4.44			6890	7090	7110	7280 \pm 110
089781	0.04	0.00	7090	4.03			7050	7180	7110	7060 \pm 130
099267	0.00	0.00	7050	4.01			7110	7030	7060	7060 \pm 100
099329	0.00	0.00	7070	4.02	6940	4.23	7000	6940	6990	6870 \pm 100
104860	0.03	0.00	5920	4.65			6000	5970	5960	6160 \pm 110
106103	0.00	0.00	6710	4.45	6650	4.55	6690	6590	6660	6530 \pm 100
107192	0.00	0.01	7090	4.26	7010	4.46	6910	6830	6960	7050 \pm 160
109032	0.00	0.00	7180	4.31			7070	7030	7090	7040 \pm 120
109799	0.00	0.00	7020	4.07	6940	4.33	7060	6830	6960	6870 \pm 150
109838	0.02	0.00	7060	4.12			7250	7170	7160	7000 \pm 250
110379	0.00	0.00	7240	4.06			6850	5720	6600	6730 \pm 300
112429	0.00	0.00	7210	4.20	7200	4.40	7280	7030	7180	7010 \pm 100
118388	0.01	0.01					6590	6230	6410	6540 \pm 250
126516	0.01	0.00	6630	4.38			6540	6350	6510	6520 \pm 250
130173	0.00	0.01	6430	3.77			6610	6450	6500	6570 \pm 200
155154	0.00	0.00	7170	4.04			7160	7130	7150	7080 \pm 140
165645	0.00	0.00	7320	4.02			7440	7220	7330	7160 \pm 160
169577	0.15	0.03	7050	4.24			7400	7350	7270	7190 \pm 300
187353	0.00	0.03	7020	4.10			7000	7040	7020	7040 \pm 300
206043	0.00	0.00	7180	4.05			7110	6830	7040	7200 \pm 120
075202	0.00	0.01	8180	4.06	7840	4.21	7890	7680	7900	8130 \pm 250
091201	0.01	0.01	7070	4.10			7090	6980	7050	6960 \pm 350
103257	0.00	0.00	6890	3.90			7100	6940	6980	6960 \pm 100
113357	0.01	0.01	7150	4.26			7100	6900	7050	6930 \pm 300
133803	0.01	0.02	7140	4.12			6940	7030	7040	7000 \pm 150
137785	0.00	0.00	7110	4.06			7050	6820	7000	6900 \pm 250
149989	0.00	0.00	7180	4.08	7070	4.43	7210	7040	7120	7000 \pm 100
188032	0.00	0.00	7230	4.20	7080	4.47	7200	7130	7160	6900 \pm 200
197451	0.01	0.02	7370	3.93			6900	7130	7130	7050 \pm 300
206481	0.00	0.00	7150	4.24	7010	4.52	6950	7040	7040	6760 \pm 150
224288	0.00	0.00	7140	4.22	6940	4.40	7040	6810	6980	6770 \pm 120
112934	0.00	0.00	7120	4.14	7150	4.56	7220	7080	7140	6900 \pm 160
115466	0.00	0.00	6970	3.93			6960	6940	6960	7200 \pm 130
124248	0.00	0.00	7220	4.16			7220	7100	7180	7400 \pm 130
171834	0.00	0.00	6720	4.03	6750	4.37	6950	6680	6780	6780 \pm 200
172416	0.00	0.00	6590	4.13	6290	3.68	6400	6200	6370	6445 \pm 100
175337	0.00	0.00	7090	4.14			6900	7090	7030	7290 \pm 160
187028	0.00	0.00	7270	4.34	7090	4.47	7240	7010	7150	6920 \pm 150
209295	0.00	0.00	7510	4.97	7470	4.25	7470	7480	7480	7110 \pm 220
216910	0.00	0.00	7070	4.07	6930	4.27	6950	6880	6960	7390 \pm 150
224638	0.00	0.00	7140	4.06			7160	6960	7090	6940 \pm 200
224945	0.00	0.00					7268	7238	7250	7300 \pm 160
041448	0.00	0.00	7240	4.13			7170	7180	7200	7290 \pm 150

* Represents the average values of effective temperature obtained from different photometric systems.

Table 4. Atmospheric parameters obtained from the hydrogen and iron lines analysis.

HD number	$T_{\text{eff}}^{H\text{lines}}$ (K)	$T_{\text{eff}}^{Fe\text{lines}}$ (K)	$\log g^{Fe\text{lines}}$ (dex)	ξ (km/s)	$v \sin i$ (km/s)	$\log \epsilon$ (Fe) (dex)
009365	7000 ± 170	7200 ± 100	3.9 ± 0.1	2.7 ± 0.2	77 ± 1	7.39 ± 0.22
019655	7000 ± 210	7100 ± 100	4.1 ± 0.3	2.8 ± 0.4	222 ± 5	7.32 ± 0.23
021788	6600 ± 140	6700 ± 100	4.1 ± 0.2	2.2 ± 0.1	13 ± 1	7.26 ± 0.21
022702	7000 ± 190	7200 ± 200	4.2 ± 0.2	2.5 ± 0.3	146 ± 2	7.40 ± 0.24
023005	7100 ± 150	7000 ± 100	3.9 ± 0.1	2.4 ± 0.1	48 ± 1	7.61 ± 0.21
023585*	7300 ± 250	7200 ± 200	4.1 ± 0.2	2.8 ± 0.3	113 ± 3	7.40 ± 0.24
026298*	6700 ± 150	6700 ± 100	4.1 ± 0.1	2.0 ± 0.2	53 ± 2	7.20 ± 0.22
033204*	7500 ± 230	7600 ± 200	4.0 ± 0.1	3.1 ± 0.1	36 ± 2	7.97 ± 0.26
046304*	7300 ± 260	7400 ± 100	4.0 ± 0.1	3.0 ± 0.4	242 ± 12	7.31 ± 0.27
063436*	7000 ± 170	7000 ± 100	3.9 ± 0.1	1.7 ± 0.2	70 ± 1	7.45 ± 0.22
089781	7000 ± 180	7200 ± 100	4.2 ± 0.2	1.3 ± 0.2	120 ± 3	7.45 ± 0.23
099267	7000 ± 170	7000 ± 100	4.2 ± 0.2	2.9 ± 0.3	100 ± 2	7.46 ± 0.23
099329*	6900 ± 200	7100 ± 200	4.1 ± 0.2	2.6 ± 0.3	142 ± 2	7.49 ± 0.24
104860	6100 ± 140	6000 ± 100	4.4 ± 0.2	1.9 ± 0.1	16 ± 2	7.34 ± 0.21
106103*	6600 ± 150	6700 ± 100	4.1 ± 0.2	1.3 ± 0.1	21 ± 1	7.40 ± 0.21
107192	6900 ± 160	7000 ± 100	3.9 ± 0.2	2.8 ± 0.2	69 ± 1	7.32 ± 0.22
109032	7000 ± 170	7000 ± 100	4.2 ± 0.2	2.6 ± 0.2	100 ± 1	7.42 ± 0.22
109799*	6900 ± 140	7000 ± 100	4.0 ± 0.1	1.8 ± 0.1	39 ± 2	7.51 ± 0.21
109838	7000 ± 140	6900 ± 100	4.2 ± 0.1	1.5 ± 0.1	13 ± 1	7.46 ± 0.21
110379*	7000 ± 150	7100 ± 100	4.1 ± 0.1	1.8 ± 0.2	34 ± 6	7.37 ± 0.21
112429	7100 ± 170	7200 ± 100	3.9 ± 0.2	3.0 ± 0.2	120 ± 3	7.29 ± 0.23
118388	6800 ± 170	6700 ± 100	4.1 ± 0.2	1.9 ± 0.2	121 ± 8	7.27 ± 0.22
126516*	7000 ± 140	6800 ± 200	4.2 ± 0.2	1.5 ± 0.2	5 ± 1	7.50 ± 0.23
130173	6700 ± 160	6800 ± 200	4.0 ± 0.2	2.2 ± 0.2	62 ± 3	7.28 ± 0.23
155154	7100 ± 200	7000 ± 100	4.0 ± 0.2	3.0 ± 0.3	183 ± 6	7.30 ± 0.22
165645	7200 ± 180	7300 ± 200	4.1 ± 0.1	3.2 ± 0.2	152 ± 4	7.36 ± 0.28
169577	7000 ± 160	7100 ± 200	4.2 ± 0.1	1.8 ± 0.2	62 ± 4	7.79 ± 0.23
187353	7300 ± 230	7200 ± 100	4.1 ± 0.1	1.7 ± 0.1	35 ± 2	7.36 ± 0.22
206043	7200 ± 190	7200 ± 200	4.0 ± 0.2	2.5 ± 0.2	135 ± 5	7.50 ± 0.23
075202	7700 ± 260	7900 ± 200	4.2 ± 0.2	0.4 ± 0.2	104 ± 2	7.51 ± 0.26
091201	7100 ± 150	7100 ± 100	3.8 ± 0.2	2.3 ± 0.1	50 ± 1	7.50 ± 0.18
103257	6900 ± 160	7100 ± 200	4.0 ± 0.2	2.3 ± 0.2	70 ± 2	7.31 ± 0.20
113357	7000 ± 160	7100 ± 100	4.1 ± 0.1	2.9 ± 0.2	67 ± 1	7.28 ± 0.19
133803	7000 ± 170	7000 ± 100	4.2 ± 0.3	2.2 ± 0.2	92 ± 2	7.37 ± 0.18
137785	7000 ± 170	6900 ± 100	3.8 ± 0.2	2.8 ± 0.2	109 ± 3	7.16 ± 0.18
149989	7000 ± 190	7100 ± 100	4.0 ± 0.2	2.8 ± 0.2	140 ± 6	7.09 ± 0.19
188032	7000 ± 160	7100 ± 100	4.0 ± 0.1	2.5 ± 0.2	54 ± 2	7.34 ± 0.18
197451	7400 ± 230	7300 ± 200	4.0 ± 0.1	3.1 ± 0.2	26 ± 3	7.73 ± 0.22
206481	6900 ± 170	6900 ± 100	4.1 ± 0.2	1.5 ± 0.2	86 ± 2	7.36 ± 0.18
224288	7100 ± 150	7100 ± 200	3.9 ± 0.1	2.2 ± 0.2	48 ± 2	7.39 ± 0.19
112934	7000 ± 170	7100 ± 100	3.9 ± 0.2	2.4 ± 0.2	75 ± 2	7.03 ± 0.22
115466	6800 ± 150	7100 ± 100	4.0 ± 0.2	2.0 ± 0.2	40 ± 3	7.56 ± 0.20
124248	7000 ± 150	7100 ± 100	4.1 ± 0.1	1.7 ± 0.2	50 ± 3	7.37 ± 0.20
171834	6700 ± 170	7000 ± 100	4.0 ± 0.2	2.7 ± 0.2	72 ± 2	7.40 ± 0.21
172416	6400 ± 150	6400 ± 100	3.9 ± 0.1	1.9 ± 0.2	55 ± 3	7.41 ± 0.20
175337	6900 ± 150	7100 ± 100	4.0 ± 0.1	1.7 ± 0.1	38 ± 2	7.73 ± 0.19
187028	6900 ± 170	7300 ± 200	4.5 ± 0.2	2.3 ± 0.3	87 ± 3	7.23 ± 0.23
209295*	7400 ± 170	7300 ± 100	4.2 ± 0.1	2.3 ± 0.2	89 ± 5	7.07 ± 0.21
216910	6900 ± 180	7100 ± 100	4.3 ± 0.2	2.1 ± 0.2	95 ± 4	7.66 ± 0.21
224638	6900 ± 140	7000 ± 100	4.0 ± 0.1	1.5 ± 0.2	29 ± 7	7.39 ± 0.20
224945	7000 ± 150	7300 ± 100	4.2 ± 0.1	2.3 ± 0.2	58 ± 2	7.39 ± 0.23
041448	7300 ± 170	7200 ± 100	4.1 ± 0.2	2.8 ± 0.2	104 ± 3	7.35 ± 0.18

* Previously determined spectroscopic atmospheric parameters:

HD23585: $T_{\text{eff}}=7440$ K, $\log g=4.29$, $\xi=3.0$ km s⁻¹ (Gray, Graham, & Hoyt 2001)

HD26298: $T_{\text{eff}}=6790 \pm 200$ K, $\log g=3.95 \pm 0.22$, $\xi=1.5 \pm 0.5$ km s⁻¹, **HD110379:** $T_{\text{eff}}=7140 \pm 160$ K, $\log g=4.21 \pm 0.02$, $\xi=1.5 \pm 0.4$ km s⁻¹, **HD126516:** $T_{\text{eff}}=6590 \pm 120$ K, $\log g=4.01 \pm 0.15$, $\xi=1.9 \pm 0.3$ km s⁻¹ (Bruntt, De Cat, & Aerts 2008)

HD33204: $T_{\text{eff}}=7646$ K, $\log g=4.11$, $\xi=3.4$, (Varenne & Monier 1999)

HD46304: $T_{\text{eff}}=7048 \pm 16$ K, **HD63436:** $T_{\text{eff}}=6970$ K, $\log g=4.14$, **HD106103:** $T_{\text{eff}}=6610$ K (Muñoz Bermejo, Asensio Ramos, & Allende Prieto 2013)

HD99329: $T_{\text{eff}}=6990$ K, **HD112934:** $T_{\text{eff}}=7035$ K, **HD209295:** $T_{\text{eff}}=7392$ K (Ammler-von Eiff & Reiners 2012)

HD109799: $T_{\text{eff}}=6926 \pm 26$ K (King & Schuler 2005)

Table 5. The average abundances and standard deviations of individual elements of the stars. Number of the analysed parts is given in the brackets. The full table is available in the electronic form.

Elements (Atomic number)	HD 9565	HD 19655	HD 21788	HD 22702	HD 23005
C (6)	8.48 ± 0.15 (7)	8.34 ± 0.24 (2)	8.52 ± 0.21 (19)	8.65 ± 0.01 (3)	8.11 ± 0.27 (8)
N (7)			8.61 ± 0.19 (1)		
O (8)			8.57 ± 0.19 (2)		
Na (11)	5.62 ± 0.14 (2)	6.65 ± 0.24 (1)	6.08 ± 0.05 (4)	6.25 ± 0.13 (1)	6.47 ± 0.28 (2)
Mg (12)	7.64 ± 0.09 (8)	7.57 ± 0.01 (4)	7.51 ± 0.22 (11)	7.69 ± 0.15 (5)	7.86 ± 0.20 (8)
Si (14)	7.21 ± 0.30 (16)	6.48 ± 0.35 (4)	7.09 ± 0.43 (40)	6.94 ± 0.32 (6)	7.15 ± 0.35 (21)
S (16)	7.29 ± 0.14 (2)		7.20 ± 0.12 (8)		7.41 ± 0.28 (2)
Ca (20)	6.48 ± 0.19 (19)	6.32 ± 0.16 (4)	6.38 ± 0.20 (32)	6.29 ± 0.06 (4)	7.01 ± 0.30 (27)
Sc (21)	2.94 ± 0.12 (10)	3.44 ± 0.24 (5)	3.20 ± 0.07 (8)	3.52 ± 0.13 (2)	3.47 ± 0.30 (12)
Ti (22)	4.94 ± 0.11 (23)	4.94 ± 0.04 (7)	4.95 ± 0.23 (92)	4.85 ± 0.16 (9)	4.93 ± 0.23 (36)
V (23)	4.94 ± 0.14 (2)		3.88 ± 0.21 (10)		4.26 ± 0.50 (4)
Cr (24)	5.56 ± 0.07 (15)	5.59 ± 0.15 (7)	5.48 ± 0.23 (85)	5.57 ± 0.06 (3)	5.64 ± 0.44 (39)
Mn (25)	5.03 ± 0.33 (8)	4.85 ± 0.24 (1)	4.94 ± 0.25 (21)	5.17 ± 0.13 (2)	5.30 ± 0.19 (8)
Fe (26)	7.39 ± 0.06 (40)	7.32 ± 0.04 (9)	7.26 ± 0.14 (299)	7.40 ± 0.13 (15)	7.61 ± 0.12 (127)
Co (27)			4.40 ± 0.21 (6)		5.37 ± 0.28 (4)
Ni (28)	6.13 ± 0.08 (16)	6.03 ± 0.08 (3)	5.94 ± 0.16 (88)	6.20 ± 0.13 (2)	6.41 ± 0.20 (23)
Cu (29)	3.56 ± 0.14 (2)		3.52 ± 0.24 (3)		4.11 ± 0.28 (1)
Zn (30)			4.18 ± 0.19 (1)		
Sr (38)	3.06 ± 0.14 (1)		3.73 ± 0.19 (1)	2.39 ± 0.13 (1)	3.92 ± 0.28 (2)
Y (39)	2.31 ± 0.13 (4)	1.92 ± 0.24 (2)	2.34 ± 0.10 (10)	2.61 ± 0.13 (2)	3.17 ± 0.23 (6)
Zr (40)	2.43 ± 0.14 (2)	2.62 ± 0.24 (1)	2.92 ± 0.21 (12)	2.80 ± 0.13 (2)	3.16 ± 0.28 (2)
Ba (56)	2.27 ± 0.16 (3)	2.98 ± 0.24 (2)	2.95 ± 0.15 (4)	2.57 ± 0.13 (2)	2.77 ± 0.34 (3)
La (57)			1.56 ± 0.19 (2)		2.11 ± 0.28 (2)
Ce (58)			1.79 ± 0.09 (10)		1.84 ± 0.28 (2)
Pr (59)			0.33 ± 0.19 (1)		
Nd (60)			1.54 ± 0.20 (19)		1.59 ± 0.28 (2)
Sm (62)			1.54 ± 0.19 (1)		